Wide graded potential wells: growth, electrical properties and theoretical results

Klaus Ensslin, Achim Wixforth, Mani Sundaram, John H. English, Arthur C. Gossard

Angaben zur Veröffentlichung / Publication details:

Ensslin, Klaus, Achim Wixforth, Mani Sundaram, John H. English, and Arthur C. Gossard. 1990. "Wide graded potential wells: growth, electrical properties and theoretical results." In *Growth of semiconductor structures and high-tc thin films on semiconductors*, edited by Anupam Madhukar, 66–75. Bellingham, WA: SPIE. https://doi.org/10.1117/12.20808.

Wide Graded Potential Wells : Growth, Electrical Properties and Theoretical Results

K. Ensslin, A. Wixforth, M. Sundaram, J.H. English, and A. C. Gossard
Materials Department, University of California, Santa Barbara

Abstract

Remotely doped parabolic quantum wells have been grown by MBE using a digital alloy approach to vary the Al content in the $Al_xGa_{1-x}As$ system. The monitoring of the beam fluxes as well as the measured subband separations confirm the precision of our growth technique. Using a front gate electrode we can depopulate the electrical subbands. Thus we can determine experimentally the subband separations showing close agreement with the results of our self-consistent calculations.

1. Introduction

Wide parabolic quantum wells have been realized by a high precision grading technique [1] as well as by temperature controlled growth rate variations [2]. These structures contain a high mobility quasi three-dimensional electron system (Q3DES) and reveal an approach to the hypothetical concept of jellium, a neutral medium consisting of an electron gas, which moves in a uniform positively charged background. Theoretical considerations of this construct predict a number of interesting many-body effects [3], many of which have not been observed experimentally, since it is difficult to realize jellium in a real solid, where the presence of the dopant atoms leads to charge localization at low temperatures and provides strong scattering centers in the neighborhood of the carriers.

For one and zero-dimensional systems [4] the confining potentials are often very close to a parabolic form, because they are in general dominated by electrostatic depletion effects. One of the fundamental questions in these low-dimensional systems is the relative importance of the depolarization effect versus the single particle intersubband spacings [5,6] in far-infrared experiments. The Q3DES may give an answer both experimentally [7] and theoretically [8] in the sense, that the specific form of the parabolic potential is the basic feature in these experiments.

The high precision grading technique discussed in this paper, which allows tailoring almost any given potential [9], represents an ideal tool to study the fundamental properties of a parabolic potential in general and its impact on nanometer scale electronic devices in particular.

2. Growth

Modern epitaxial growth techniques such as molecular beam epitaxy (MBE) lend themselves readily to the growth of smooth and abrupt or graded GaAs-$Al_xGa_{1-x}As$ heterointerfaces.[10] In the structures, which are the subject of this paper, electrons are introduced into wide parabolic wells by remotely doping the barrier layers surrounding the well. The parabolic potential wells themselves are created by appropriately grading the Al mole fraction x of an $Al_xGa_{1-x}As$ alloy

layer. The electrons are found to distribute themselves uniformly, their density being governed almost entirely by the curvature of the design parabola, in the limit of temperature T=0.

In the following we discuss the preparation of our parabolic wells and verify the degree of precision which can be obtained. In the GaAs-$Al_xGa_{1-x}As$ system there exists a nearly linear relationship between the $Al_xGa_{1-x}As$ energy bandgap and the Al mole fraction x for $x<0.45$. [11] Controlled variation of x results in a correspondingly controlled variation of the alloy bandgap as well as the conduction band offset between GaAs and $Al_xGa_{1-x}As$. We solve this problem by growing a superlattice with a constant period (sufficiently small to permit tunneling of the electrons between the layers), each period composed of two layers: GaAs and $Al_xGa_{1-x}As$ where x is greater than or equal to the maximum Al mole fraction in the graded alloy. The duty cycle of the $Al_xGa_{1-x}As$ is varied in a controlled manner so that the average Al mole fraction follows the desired profile [12]. In other words, the Al beam is pulsed in a controlled fashion by controlling the Al oven shutter in an MBE machine. We refer to the alloy obtained by this growth technique as a digital alloy.

The actual profile of the Al mole fraction versus depth obtained is not easily measured directly. Its general shape is sometimes deduced from optical and electrical measurements on the resulting structures [13], followed by a fitting of the data to calculations for the designed energy bandgap profile. Small discrepancies between experiment and design are accounted for through mathematically constructed variations of the actual profile from the design profile. These techniques are indirect at best. Techniques like SIMS have limited depth resolution, and are destructive besides. It is very useful, at any rate, to be able to calibrate deposited Al mole fraction versus depth before growth with a simple, reproducible technique having reasonably high resolution and accuracy.

We present such a technique. The measurements is done in the MBE machine itself in a calibration run immediately prior to the sample growth. If the variation from one measured run to another is negligibly small, the measured profile can be reasonably assumed to be the actual profile grown.

The Al flux can be measured by an ion gauge of the type that is standard in a commercial MBE machine. The beam flux monitor is used for this purpose as it can be made to directly face the ovens. The collector current (usually in the range of nA) of the ion gauge is fed to a fast pA-meter. The variation of the Al flux with time is therefore measured directly. Inasmuch as actual growth occurs in the presence of a constant Ga flux, a constant collector current corresponding to the Ga flux is assumed in the calculations. The Ga flux is adjusted to be in the same ratio to a particular Al flux as the ratio of the corresponding GaAs and AlAs growth rates, which are in turn determined by RHEED oscillations immediately prior to the ion-gauge measurements. Integrating the total flux in time gives us a measure of the thickness z of the graded alloy grown. The variation of the Al mole fraction x with depth z can therefore be measured and compared with the design profile.

The method is applicable to measuring the alloy grades of digital alloys. The Al fraction in the alloy may in places be designed to be very small. In the digital alloy technique this requires very rapid pulsing of the pneumatic shutter of the Al oven and thence of the Al beam flux. This causes corresponding rapid changes in the collector current of the ion gauge. Hence we use a fast pA-meter to track the current.

Measurements were made in a Varian Gen II machine used for the growth of the GaAs-$Al_xGa_{1-x}As$ epilayers. Oven temperatures and shutter opening times are controlled by a computer having a time resolution of 10 ms. The equation of the desired profile versus depth is used by the computer to generate a sequence of shuttering times of the Al oven pneumatic shutter, with a time resolution fine enough to produce a smooth alloy gradient. The ion gauge of the beam flux monitor faces the ovens, and is situated at the same location where the substrate would be during growth. The collector current of the beam flux monitor is measured with a pA-meter whose analog output is fed back to the controller. All computations are then performed by the controller at the end of the run. More experimental details are included in Ref. 9. This described procedure allows a precise calibration of the opening and closing times of the Al shutter to provide a precise parabolic profile of the potential well.

For a comparison, the growth of two parabolic wells, one grown in the analog way by varying the temperature of the Al oven [2] and the other digital [1], both 200 nm wide and with the Al mole fraction going from 0.01 (1%) at the center of the well to 0.3 (30%) at the well-edges, is then run, and the corresponding ion-gauge profiles are presented together with the ideal design profile in the top half of Fig. 1. The deviations Δx_{Al}, from the ideal profile are plotted in the bottom half, and are seen to be < 0.02 in the case of the digital alloy and < 0.03 for the analog alloy. The maximum Al oven temperature in either case is one that gave an AlAs growth rate of 0.32 μm/hour. The superlattice period is 2 nm for the digital alloy; for the analog alloy, the temperature of the Al oven is changed at a variable rate, each time interval corresponding to the time required to grow 2 nm of alloy material at the particular Al oven temperature. The Al flux is measured every 10 ms and integrated so that the average Al mole fraction is plotted with the same resolution as the period, in this case 2 nm.

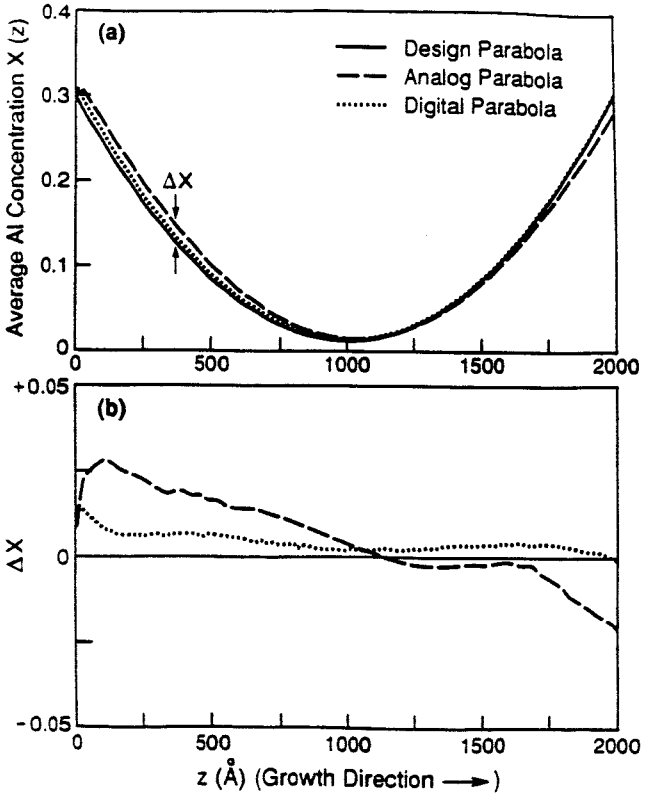

Figure 1:
Measured Al mole fraction versus depth profiles for a 200 nm wide parabolic well with Al mole fraction going from 1% at the center to 30% at the edges, grown with both the pulsed Al beam (digital alloy), and the variable Al oven temperature (analog alloy) methods. The design profile is also shown for comparison. A constant background GaAs growth rate of 0.75 μm/hour is assumed. Bottom half shows deviations of both measured alloy grades from design parabola.

The shift of the analog profile from the ideal profile observed is a result of the limits of cooling and heating rates of the Al charge. The Al charge is cooled simply by thermal conduction and radiation and has therefore a certain maximum cooling rate. Sufficient controllability of the negative gradient of Al mole fraction versus time is still possible even with a high constant background GaAs growth rate of 0.75 μm/h, as manifested by the measured analog-alloy parabolic well. In the case of the digital alloy the resolution of this measurement technique is ultimately limited by the resolution and the speed of the pA-meter. The overall accuracy of the actual graded alloy grown is still limited by the 3% accuracy of the measurement of GaAs and AlAs growth rates by the RHEED oscillation method.

We have presented a direct technique to measure graded $Al_xGa_{1-x}As$ alloy deposition profiles versus depth with a high degree of precision. Using this method we have further shown, that our grown parabolic quantum wells are of very high quality and that our digital alloy approach produces so far the best available parabolic profiles. The method is applicable to measuring the alloy grades of other III-V ternary alloys, especially where critical composition control is required to avoid misfit dislocations in the growth of strained graded alloys.

3. Capacitance Measurements

The potential of a parabolic quantum well (PBW) can be mimicked by a spatially uniform, three-dimensional (3D) slab of positive charge, which is directly related to the curvature of the parabola, namely

$$n^+ = \frac{\varepsilon\,\varepsilon_0}{e^2}\frac{\partial^2 E_c}{\partial z^2} = \frac{8\,\varepsilon\,\varepsilon_0 \Delta}{e^2 w^2}$$

Here, $\varepsilon\varepsilon_0$ is the mean dielectric constant of $Al_xGa_{1-x}As$, Δ is the energetic height of the parabola from its bottom to its edges, e is the electronic charge, w is the width of the parabolic well and E_c is the potential of the bottom of the conduction band in the region of the well. Mobile electrons provided through remote doping, then act to screen this fictitious charge, forming a Q3DES of nearly uniform density and high mobility due to the absence of charged scattering centers. If the well is completely filled, the electron density exactly equals the density n^+ and the resulting potential is that of a rectangular well with flat bottom. [1,15,16,17] Since the potential can be chosen to be very wide, quantization effects play only a minor role and many electric subbands are occupied.

Similar to Si-MOS structures [14] it is now possible to change and deplete the charge density by an electric field along the growth direction. In our structures, however, due to the large extent of the charge distribution within the PBW, the electric field leads to a shift of the charge density and a successive depopulation of subbands. Experimentally, we apply the electric field via a front gate, which is evaporated in a circular geometry on top of the sample, and ohmic contacts to the conducting channel of electrons. The capacitance between these two electrodes is measured by conventional lock-in techniques with frequencies between 10 Hz and 1000 Hz at liquid He temperatures T=4.2 K. No significant frequency dependence of the capacitance has been observed in this range.

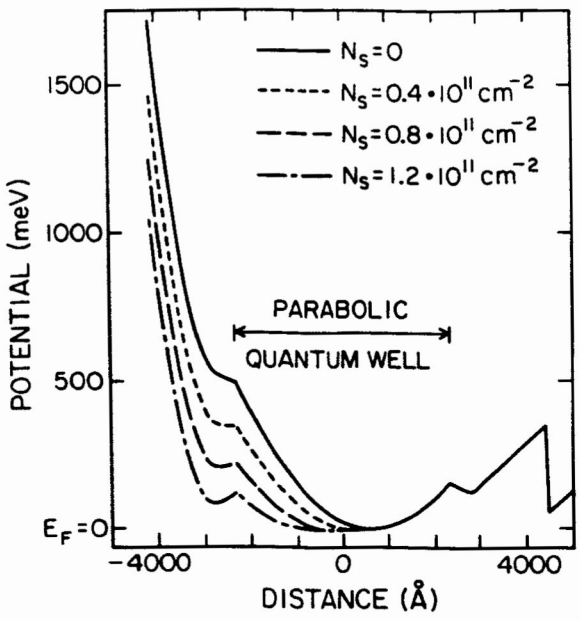

Figure 2;
Self-consistently calculated potential for different carrier densities. The plot displays the overall potential from the gate, which is on the left hand side of the figure, to the substrate, being on the right hand side. For increasing carrier density the well becomes flat due to the screening of the electrons and the center of the potential moves towards the front gate.

In the following we wish to report on the results obtained in a nominally 464 nm wide parabolic $Al_xGa_{1-x}As$ well with $0<x<0.3$. Figure 2 shows the conduction band of the PBW for different values of the applied gate voltage and therefore different carrier densities N_S. The curves represent results from a self-consistent calculation as described in the next chapter. For increasing N_S the parabola becomes more and more screened out by the electrons and the center of the potential well moves towards the front gate.

In Fig. 3 we present the experimental results of the capacitance versus voltage (CV) measurements. In contrast to corresponding measurements on quasi two-dimensional samples, where the capacitance for $V_g>V_{th}$ at B=0 is nearly independent of the gate bias, the overall capacitance tends to decrease with decreasing gate voltage V_g for a parabolic well. This decrease is more pronounced the wider the well under investigation. In addition, we observe steplike changes in the capacitance at specific values of V_g. At $V_g=V_{th}$, the Q3DES becomes depleted, indicated by a very sharp decrease in the capacitance signal. The lower trace in Fig. 3 depicts the simultaneously recorded in-phase signal, which is used to monitor the current flowing between gate and Q3DES. No such current is observed for $V_g<0$, whereas for a small positive bias a strong increase in this current occurs. This indicates the alignment of the Fermi level with the donor levels in the $Al_xGa_{1-x}As$, resulting in a conducting layer between gate and Q3DES. The absolute values of the measured capacitances have been calibrated by use of known capacitors.
Using a mean dielectric constant of 12.5 for the layers between the gate electrode and the leading edge of the Q3DES, the measured capacitance at $V_g=0$ agrees very well with the one calculated in simplest approximation, using the known thickness d=180 nm between the gate electrode and the edge of the MBE grown parabola, the thickness w=464 nm of the well itself, and the actual thickness w_e=225 nm of the Q3DES as defined above. The capacitance at $V_g=0$ thus is determined by the thickness $d_{tot}=d+(w-w_e)/2$ between the gate electrode and the leading edge of the Q3DES. The total capacitance per unit area in our samples is then expected to be given by three terms [18,19], namely

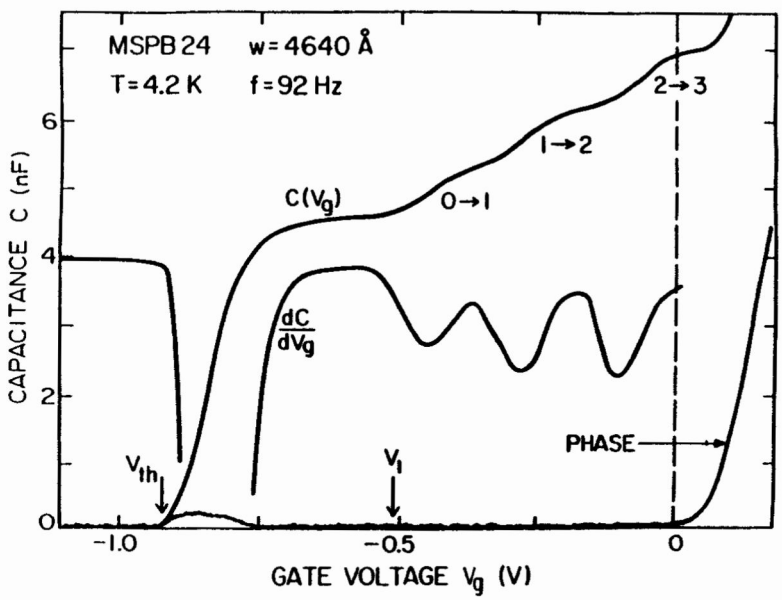

Figure 3:
Experimentally obtained capacitance versus gate voltage for a nominally 464 nm wide parabolic well. With decreasing gate voltage, the well is depleted of mobile carriers, leading to a decrease in the effective thickness of the quasi three-dimensional electron system, which in turn results in a decreasing capacitance. At particular gate voltages subsequent subbands become depopulated, as indicated by steps in the $C(V_g)$ curve. These steps are more clearly visible in the differential capacitance dC/dV_g.

The transition from subband 0 to subband 1 marks the transition from quasi 2D to quasi 3D behavior of the electron system. The simultaneously recorded signal which is in phase with the applied ac-voltage, indicates no perpendicular conductance of the sample for gate voltages $V_g<0$ and demonstrates that the signal is purely capacitive. Both the phase signal as well as the differential capacitance are given in arbitrary units.

$$\frac{1}{C_{tot}} = \frac{1}{C_{ins}} + \frac{1}{C_{PBW}} + \frac{1}{e^2 \Sigma \partial n_i / \partial \mu_i}$$

Here, e is the electronic charge, n_i is the carrier density in the i-th subband and μ_i is the corresponding chemical potential. The first two terms describe the contribution of the geometrical capacitance of the dielectric insulating layer between the gate electrode and the leading edge of the Q3DES in the parabolic well, given by

$$C_{ins} = \frac{\varepsilon \varepsilon_0}{d} \qquad \text{and} \qquad C_{PBW} = \frac{\varepsilon \varepsilon_0}{\{(w-w_e)/2\} + z_0}$$

In these expressions, ε and ε_0 are the electric permitivities of the semiconductor and the vacuum and d, w, and w_e the thicknesses of the layers defined above. The most important difference from the simple 2D case is the expression for C_{PBW}, taking into account the actual spatial width of the electron system. Here, the leading edge of the Q3DES is defined by the point where

$$N(z) = \Sigma N_s^i |\xi_i|^2$$

drops to half its maximum value. Application of a negative bias tends to shift the bottom of the parabola and thus the center of the wavefunctions to $z=z_0$, a fact which also has to be included in the calculation of the capacitance. The third term contains the thermodynamic density of states [19] at the Fermi energy, if several occupied subbands are taken into account. We interpret the decrease in capacitance with decreasing gate voltage in terms of two effects. First, while the channel is being depleted of electrons, the width w_e of the Q3DES decreases, resulting in a decrease in C_{PBW}. This is unique to the Q3DES and is due to a decreasing sheet carrier concentration whereas the space charge density remains constant. Our experiments thus yield a first direct observation of this shrinkage in the width of a Q3DES as a function of the carrier density. Secondly, a negative bias of the gate electrode with respect to the channel shifts the bottom of the effective potential and thus the centers of the wavefunctions with respect to the bottom of the MBE grown parabola to the depth z_0, as previously shown in Fig. 2. Both effects result in an increase of the effective thickness of the dielectric layer between gate and Q3DES and thus in a decrease of the measured capacitance. The value for the measured capacitance just above inversion threshold, i.e. shortly before the channel becomes depleted and $w_e(V_{th})=0$, reveal a total change in thickness of $\Delta d = w_e(V_{th})/2 + z_0 = 185$ nm. In this model, the center of the wavefunctions thus has been shifted by approximately 70 nm between $V_g=0$ and $V_g=V_{th}$, based on purely geometrical considerations and the measured capacitance. We observe no qualitative difference of the capacitance measurements on digital or analog parabolic wells.

We attribute the steps in the capacitance at particular gate voltages to a direct image of the subband structure within the well. Depleting the channel is accompanied by a successive electrical depopulation of these subbands, and thus by steplike changes in the density of states, leading to steplike changes in the third term of the capacitance equation. In addition, the effective width of the Q3DES changes also in a steplike way, since the leading edge according to its definition changes rapidly, once a subband becomes depopulated and the character of the wavefunction changes. The occurrence of three steps in the capacitance besides the large one at $V_g=V_{th}$ leads to the conclusion that four subbands are occupied at $V_g=0$ and become successively depopulated with application of a negative gate bias. Thus we are able to directly observe the electric depopulation of subbands in a high quality Q3DES with up to four subbands occupied.

4. Self-consistent Calculations

The PBW system constitutes a crucial test for self-consistent subband calculations, since the shape of the potential is qualitatively changed due to the presence of the electrons. This is in contrast to the triangular shaped potential in heterostructures, where the subband separations are only quantitatively increased by self-consistent effects. [20,21] We solved Poisson and Schroedinger equations self-consistently according to the recipes given in the literature. [20,21,22] Figure 4 presents the results of this calculation for three different carrier densities. In contrast to Fig. 2 only the parabolic part of the potential is shown. The problem is treated by explicitly taking into account the almost parabolical spatially varying effective mass inside the PBW according to the modified Hamiltonian described by Ref. 23. However, we find, that the subband energies differ by less than 0.1 meV, when being calculated with a constant value of $m^* = 0.067\ m_0$, corresponding to the band edge mass of GaAs, compared to the parabolically varying mass. This is due to the fact, that the wavefunctions and thus the probability of the electrons to stay in the regions of high Al content is very low. The scale in z-direction is chosen thus that $z=0$ corresponds to the center

of the as-grown parabola. Figure 4 shows, that the center of the electron distribution shifts with respect to z=0.

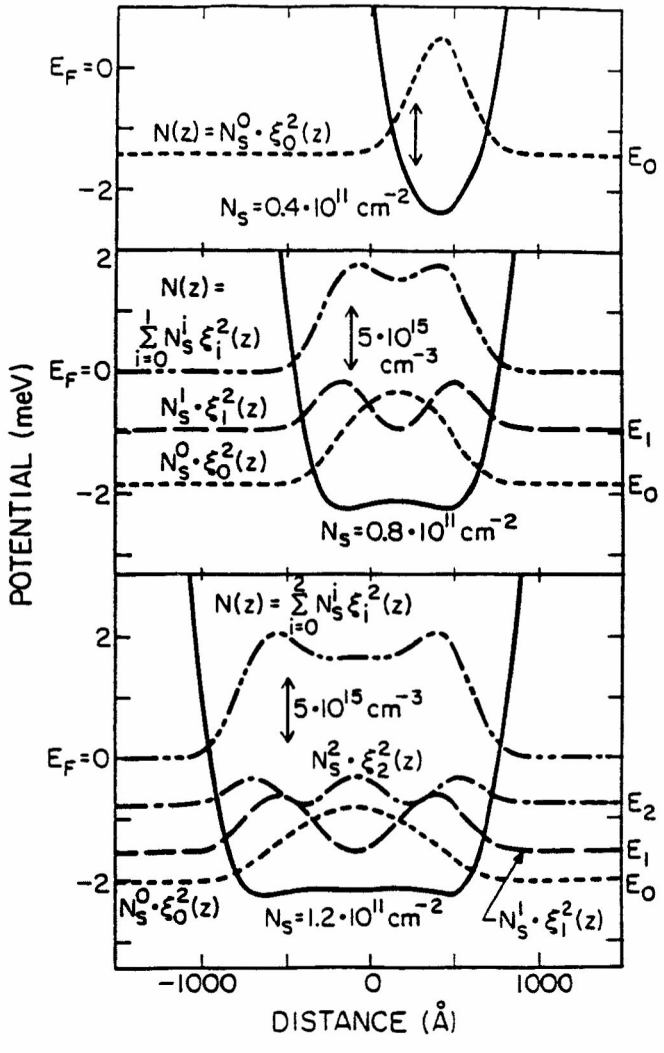

Figure 4:
Calculated self-consistent potential for a quasi three-dimensional electron system in a parabolic quantum well of thickness w=464 nm. The potential and the probability amplitudes of the electron distributions are shown for three different carrier densities within the well. Increasing carrier density leads to a flattening of the bottom of the well and to an increase in the thickness of the electron distribution, whereas the intersubband separations decrease. Typical subband energies are of the order of meV.

In Fig. 5 the carrier densities N_S^i and energies of the various subbands are plotted as a function of gate voltage. Even though the absolute voltage scale in the figure does not exactly coincide with the one in the experiment (see Fig. 3) due to the not precisely known concentration of ionized donors, the calculation predicts a fourth subband to become occupied at a total carrier density N_S = 1.3 x 10^{11} cm^{-2}, which is in good agreement with the experiment. The subband separations in this case are consistent with those expected for a wide rectangular well, i.e. the subband energies E_i vary as i^2 with the lowest one of the order of 0.3 meV. This proves the concept of quasi-doping, tending towards a quasi uniform electron distribution as represented in a rectangular Hartree potential. At $V_g=V_1$, only one subband remains occupied and the system undergoes the transition from quasi 3D to quasi 2D at this particular gate voltage. In the calculation as shown in the lower part of Fig. 5 this transition is indicated by a linear dependence of (E_F-E_0) on N_S for voltages $V_{th}<V_g<V_1$, as expected for a 2DES. For voltage $V_g > V_1$ however, (E_F-E_0) remains nearly constant, in agreement with the concept of a Q3DES.

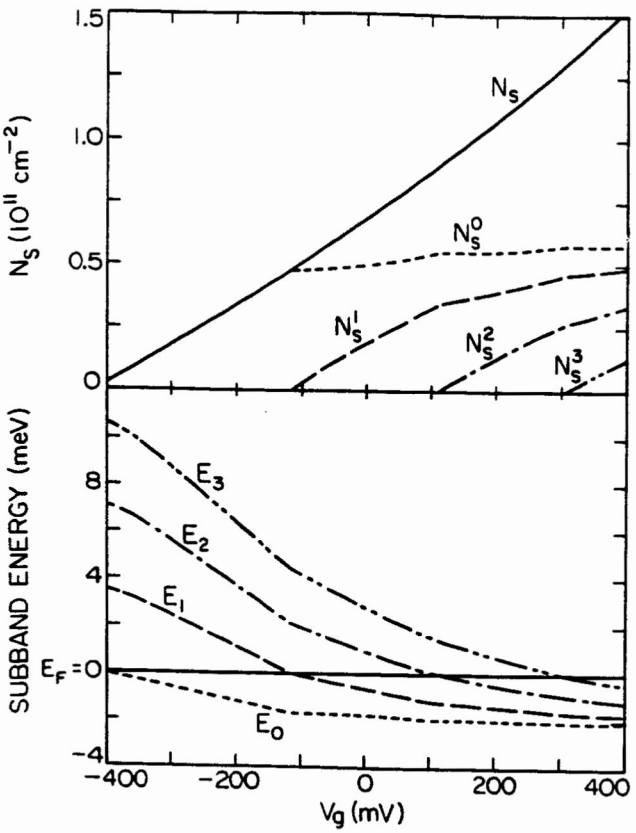

Figure 5:
Calculated carrier density and subband separation as a function of the applied gate voltage V_g for a 464 nm wide parabolic quantum well. At a total carrier density of N_S = 1.3x10^{11} cm^{-2} four electrical subbands are occupied. The subband energies change from those of an harmonic oscillator in the empty well to those of a rectangular square well for the partially filled well. In the region, where only one subband is occupied, the system behaves quasi two-dimensionally, as indicated by a linear dependence of (E_F-E_0) on N_S, whereas for higher carrier densities (E_F-E_0) remains nearly constant.

We thus are able to directly calculate the expected capacitance as a function of gate voltage, combining both the geometrical considerations and the results of our self-consistent calculations. The overall trend of a decreasing capacitance can clearly be demonstrated, whereas the magnitude of the steps at gate voltages where subsequent subbands become populated, is underestimated by the calculations by a factor of the order of five and thus not as developed as in the experiment. The voltages at which the steps in the capacitance occur, however, are in good agreement with the ones obtained in the experiment, taking into account a fixed offset in the gate voltage, as discussed above. The height of the steps in the capacitance depends strongly on the actual population process of the subbands, which can be influenced by exchange and correlation effects [21,22,24]. In addition it is not clear how localized states are contributing to the capacitance signal. Especially for low carrier densities N_S^i most of the carriers can be localized. The localization of the carriers might be due to higher harmonics of the potential or alloy disorder. These effects lead to an increase of the dN_S^i/dV_g slope and can thus enhance the steps in the capacitance signal.

5. Conclusions

We have grown wide parabolic quantum wells using a digital alloy approach. A direct method to monitor the Al distribution inside the well is presented and reveals the high quality of the parabolic profiles in our structures. By using a front gate electrode we can deplete the electron gas with an electric field. The shift of the electron distribution inside the well as well as its shrinkage for decreasing carrier density are directly observed in the gate versus channel capacitance. In addition, we find steps in the capacitance signal, which are directly related to the successive depopulation of subbands. The energetic position of the steps agrees nicely with the results of a

self-consistent subband calculation. The surprising height of the steplike changes in the capacitance remains to be explained. The possibility of tuning the dimensionality of the electron system promises very interesting results on the way to study residual three-dimensional effects in lower dimensional systems.

6. Acknowledgements

We gratefully acknowledge fruitful discussions with Beth Gwinn, Bob Westervelt and Louis Brey. This work was supported in part by the U.S.Air-Force Office of Scientific Research and QUEST, an N.S.F. Science and Technology center.

7. References

1. M. Sundaram, A. C. Gossard, J. H. English, and R. M. Westervelt, Superlattices and Microstructures **4**, 683 (1988)
2. M. Shayegan, T. Sajoto, M. Santos, and C. Silvestre, Appl. Phys. Lett. **53**, 791 (1988)
3. see e.g. B. I. Halperin, Jap. Journal Appl. Phys. **26**, 1913 (1987)
4. For a recent review see:
   Physics and Technology of Submicron Structures, edited by H. Heinrich, G. Bauer, and F. Kuchar, Springer Series in Solid State Sciences Vol.83, 1988
5. F. Brinkop, W. Hansen, J. P. Kotthaus, and K. Ploog, Phys, Rev. **B37**, 6547 (1988)
6. Ch. Sikorski and U. Merkt, Phys. Rev. Lett. **62**, 2164 (1989)
7. K. Karrai, X. Ying, H. D. Drew, and M. Shayegan, Phys. Rev. **B40**, 12020 (1989)
8. L. Brey and N. Johnson, Phys. Rev. **B40**, 10647 (1989)
9. M. Sundaram, A. Wixforth, R. S. Geels, A. C. Gossard, and J. H. English, to be published
10. A. C. Gossard, J. Quant. Electronics, **QE-22**, #9, 1649 (1986)
11. S. Adachi, J. Appl. Phys. **58**, R1 (1985)
12. M. Kawabe, M. Kondo, N. Matsuura, and K. Yamamoto, Jpn. J. Appl. Phys. **22**, L64 (1983)
13. R. C. Miller, A. C. Gossard, D. A. Kleinmann, and O. Munteanu, Phys. Rev. **B29**, 3740 (1984)
14. T. Ando, A. B. Fowler, and F.Stern, Rev. Mod. Phys.**54**,437 (1982)
15. E. G. Gwinn, R. M. Westervelt, P. F. Hopkins, A. J. Rimberg, M. Sundaram, and A. C. Gossard, Phys. Rev. **B39**, 6260 (1989)
16. K. Karrai, H. D. Drew, M. W. Lee, and M. Shayegan, Phys. Rev. **B39**, 1426 (1989)
17. T. Sajoto, J. Jo, L. Engel, M. Santos, and M. Shayegan, Phys. Rev. **B39**, 10464 (1989)
18. T. P. Smith III, B. B. Goldberg, and P. J. Stiles, Phys. Rev. **B32**, 2696 (1985)
19. V. Mosser, D. Weiss, K. v. Klitzing, K. Ploog, and G. Weimann, Sol. St. Comm. **58**, 5 (1986)
20. F. Stern and S. Das Sarma, Phys. Rev. **B30**, 840 (1984)
21. T. Ando, Journ. of the Phys. Soc. of Jpn., **51**, 3893 (1982)
22. F. Stern, Phys. Rev. B5, 4891 (1972)
23. Qi-Gao Zhu and H. Kroemer , Phys. Rev. **B27**, 3519 (1983)
24. K. Ensslin, D. Heitmann, and K. Ploog, to be published in Surface Science